Wang *et al.*
Chinese Journal of Mechanical Engineering (2023) 36:78
https://doi.org/10.1186/s10033-023-00894-6

Chinese Journal of Mechanical Engineering

ORIGINAL ARTICLE

Open Access

Tribological Mechanism of Graphene and Ionic Liquid Mixed Fluid on Grinding Interface under Nanofluid Minimum Quantity Lubrication

Dexiang Wang[1,2], Yu Zhang[1,2], Qiliang Zhao[1,2], Jingliang Jiang[1,2], Guoliang Liu[1,2] and Changhe Li[1,2*]

Abstract

Graphene has superhigh thermal conductivity up to 5000 W/(m·K), extremely thin thickness, superhigh mechanical strength and nano-lamellar structure with low interlayer shear strength, making it possess great potential in minimum quantity lubrication (MQL) grinding. Meanwhile, ionic liquids (ILs) have higher thermal conductivity and better thermal stability than vegetable oils, which are frequently used as MQL grinding fluids. And ILs have extremely low vapor pressure, thereby avoiding film boiling in grinding. These excellent properties make ILs also have immense potential in MQL grinding. However, the grinding performance of graphene and ionic liquid mixed fluid under nanofluid minimum quantity lubrication (NMQL), and its tribological mechanism on abrasive grain/workpiece grinding interface, are still unclear. This research firstly evaluates the grinding performance of graphene and ionic liquid mixed nanofluids (graphene/IL nanofluids) under NMQL experimentally. The evaluation shows that graphene/IL nanofluids can further strengthen both the cooling and lubricating performances compared with MQL grinding using ILs only. The specific grinding energy and grinding force ratio can be reduced by over 40% at grinding depth of 10 μm. Workpiece machined surface roughness can be decreased by over 10%, and grinding temperature can be lowered over 50 ℃ at grinding depth of 30 μm. Aiming at the unclear tribological mechanism of graphene/IL nanofluids, molecular dynamics simulations for abrasive grain/workpiece grinding interface are performed to explore the formation mechanism of physical adsorption film. The simulations show that the grinding interface is in a boundary lubrication state. IL molecules absorb in groove-like fractures on grain wear flat face to form boundary lubrication film, and graphene nanosheets can enter into the grinding interface to further decrease the contact area between abrasive grain and workpiece. Compared with MQL grinding, the average tangential grinding force of graphene/IL nanofluids can decrease up to 10.8%. The interlayer shear effect and low interlayer shear strength of graphene nanosheets are the principal causes of enhanced lubricating performance on the grinding interface. EDS and XPS analyses are further carried out to explore the formation mechanism of chemical reaction film. The analyses show that IL base fluid happens chemical reactions with workpiece material, producing FeF_2, CrF_3, and BN. The fresh machined surface of workpiece is oxidized by air, producing NiO, Cr_2O_3 and Fe_2O_3. The chemical reaction film is constituted by fluorides, nitrides and oxides together. The combined action of physical adsorption film and chemical reaction film make graphene/IL nanofluids obtain excellent grinding performance.

Keywords Grinding, Nanofluid minimum quantity lubrication, Graphene, Tribological mechanism

*Correspondence:
Changhe Li
sy_lichanghe@163.com
Full list of author information is available at the end of the article

1 Introduction

The effective cooling and lubrication in grinding zone are of great significance to improve the surface integrity of machined workpiece. Due to existing problems of conventional flood grinding, such as low useful fluid flowrate [1], high fluid use-cost [2], and high environment and health risks [3], it is unable to satisfy the requirements of green manufacturing. Against this background, minimum quantity lubrication (MQL) technique emerges as The Times require, which possesses the advantages of high-efficiency, low-consumption, and environmentally-friendly. However, MQL technique is lack of heat exchange capability and cannot meet the cooling requirements in the grinding zone compared with flood grinding [4]. Therefore, MQL technique still needs to be continuously improved so as to take the place of flood grinding.

1.1 Applications of Graphene in NMQL Grinding

Nanofluid minimum quantity lubrication (NMQL) technique enhances the heat exchange capability of MQL technique via using solid nanoparticles. The nanoparticles have high thermal conductivity and possess small size effect and large specific surface area, and thus can strengthen the heat conduction and convection processes in the grinding zone [5]. Further researches indicate that nanofluids not only can enhance the heat exchange capability of MQL technique, but also can further improve the anti-wear and friction-reducing properties [6–8]. At present, the frequently used nanoparticles mainly include metallic and non-metallic compounds, such as Al_2O_3 [9–11], SiO_2 [9, 12], CuO [13–15], ZrO_2 [9], and MoS_2 [9, 14, 16], and carbon family materials, such as diamond [9, 17, 18], carbon nanotube (CNT) [9, 17, 19], and graphene [20–23]. The nanofluids prepared from those nanoparticles have their own different cooling and lubricating properties. Among those nanoparticles, graphene has superhigh thermal conductivity up to 5000 W/(m·K) [24], higher than other materials of carbon family and metallic materials like aluminum and copper, making graphene an ideal material for heat transfer applications. Meanwhile, graphene has extremely thin thickness that single layer thickness is just only 0.34 nm [25], making graphene easy to enter into frictional contact interface to form adsorbed film. In addition, graphene has superhigh mechanical strength that its intrinsic strength is up to 130 GPa [26], and has nano-lamellar structure with low interlayer shear strength, making the adsorbed film with high bearing capacity and low frictional coefficient. These excellent properties make graphene nanofluids possess both good heat transfer and tribological properties, and hence have immense potentials for MQL grinding applications. Those researches also confirm this viewpoint in Refs. [20–23].

1.2 Applications of Ionic Liquids in Grinding

Ionic liquids (ILs) are a class of organic salts, which are liquids with melting point close to or below room temperature. The property of being liquid at room temperature and the existence form of only ions make ILs excellent heat transfer fluids [27]. From Table 1, it can be found that ILs have higher thermal conductivity and better thermal stability compared with vegetable oils, which are frequently used as MQL grinding fluids. In addition, ILs have extremely low vapor pressure, and thus can avoid the occurrence of film boiling in the grinding zone. Further researches indicate that ILs also have outstanding lubricating property and can easily form boundary lubrication film on the contact interfaces between multiple friction pairs [33]. Because of successful applications in the field of tribology, ILs gradually attract the attention of the field of machining. Existing researches indicate that ILs exhibit better lubricating property compared with conventional oil-based cutting fluids, no matter used as cutting fluids [34] or additives [35, 36]. Benefiting from their excellent heat transfer and lubricating properties, ILs also have immense potentials in MQL grinding.

1.3 The Tribological Mechanisms of Nanoparticles on Grinding Interface under NMQL

The introduction of solid nanoparticles into grinding interface under NMQL can cause new changes to the formation mechanism of lubrication film between abrasive grain and workpiece. Currently, existing researches mainly put forward the following four tribological

Table 1 Thermophysical properties of ionic liquids and vegetable oil

Property	$[BMIM]BF_4$	$[HMIM]BF_4$	Vegetable oils
Thermal conductivity at 25 °C (W/(m·K))	0.186 [27]	0.170 [28]	<0.170 [29]
Heat capacity at 100 °C (J/(g·K))	1.66 [27]	2.68 [28]	<2.60 [29]
Density at 20 °C (g/cm^3)	1.26 [30]	1.15 [31]	<1.00 [29]
Thermal decomposition onset (°C)	403 [30]	358 [31]	About 300 [32]

mechanisms for nanoparticles [37–40]. (1) Rolling effect. Nanoparticles can transform the sliding friction between the abrasive grain and the workpiece into rolling friction. (2) Filling effect. Nanoparticles can be filled in the groove-like fractures on workpiece surface, taking the effect of repairing surface of the workpiece. (3) Polishing effect. Nanoparticles can play a polishing role between the abrasive grain and the workpiece. (4) Film effect. On one hand, chemical reaction film can be formed on the abrasive grain/workpiece grinding interface resulting from the chemical reactions between nanofluid, abrasive grain and workpiece. On the other hand, friction adsorption film can be formed resulting from the tribological behaviors of nanoparticles on the grinding interface, such as adsorption, extrusion, shear, deformation, sliding and rolling.

However, owing to the difficulties of experimentally observing the interactions between abrasive grain, workpiece and droplets, the tribological mechanism of nanofluids on the grinding interface are only speculated from SEM, AFM, and EDS analyses of the post-grinding surfaces of the workpiece and grinding wheel. Although these speculations can explain some experimental phenomenon, there are still lack of direct evidences to reveal internal mechanisms from microscale viewpoints. Systematic microscale study for abrasive grain/workpiece grinding interface is still needed to reveal the tribological mechanism of nanofluids on the grinding interface. Molecular dynamics simulation is an effective method to perform microscale research, and can investigate the interactions from atomic scale. The previous researches in Refs. [41, 42] have certified its atomic-scale computational capacity for abrasive grain/workpiece grinding interface.

To sum up, due to graphene and ILs both have excellent heat transfer and lubricating properties and both have great potential in MQL grinding, this research will firstly investigate the MQL grinding performance of graphene and ionic liquid mixed nanofluid (graphene/IL nanofluid). Secondly, molecular dynamics simulations for abrasive grain/workpiece grinding interface will be performed to explore the formation mechanism of physical adsorption film obtained from graphene/IL nanofluid. Finally, EDS and XPS analyses of post-grinding workpiece surfaces will be carried out to explore the formation mechanism of chemical reaction film. Based on the explorations, the tribological mechanism of graphene/IL nanofluid on the grinding interface will be further revealed.

2 Experimental Schemes

Grinding experiments under NMQL, MQL, flood, and dry conditions are carried out to investigate the MQL grinding performance of graphene/IL nanofluid.

2.1 Preparation of Graphene/IL Nanofluids

Two kinds of ILs are used to prepare graphene/IL nanofluids, which are 1-butyl-3-methylimidazolium tetrafluoroborate, [BMIM]BF_4, and 1-hexyl-3-methylimidazolium tetrafluoroborate, [HMIM]BF_4, respectively. The ILs are produced by Qingdao Ionike New Material Technology Co., Ltd. The graphene nanosheets have an average diameter of 1–3 μm and average thickness of 1–5 nm, purchased from Nanjing XFNANO Materials Tech Co.,Ltd. The graphene/IL nanofluids with 0.5 wt% of graphene is prepared through two-step method, as shown in Figure 1. Firstly, the quantitative graphene nanosheets and ILs are weighed using JA503A electronic analytical balance. Afterwards, the graphene nanosheets and ILs are mixed and stirred for 3 min using DF-101Z magnetic stirrer. Finally, the JP-020S ultrasonic assisted oscillator is used to oscillate for 20 min with ultrasonic power of 120 W and oscillation frequency of 40 kHz. The graphene nanosheets can be uniformly and stably dispersed in ILs via the above operations. The graphene/[BMIM]BF_4 and graphene/[HMIM]BF_4 nanofluids will be abbreviated as the GN/BB and GN/HB nanofluids in the following.

2.2 Experimental Set Up

Grinding experimental platform is built on K-P36 numerical control precision surface grinder, as shown in Figure 2. The liquid supply equipment is KINS KS-2106 supply system, and it uses high-pressure pulse airflow to drive piston pump to supply liquid. The supplied liquid will be subsequently atomized in the atomization nozzle by high pressure air, so as to form aerosol jet flow in high-speed movement. A ceramic white corundum grinding wheel is used in the experiments, of which the diameter and the width are 300 mm and 20 mm, respectively. The workpiece material is Ni-based superalloy GH4169, and the workpiece size is 40 mm × 30 mm × 30 mm. Grinding direction is along the workpiece length direction. Grinding width is equal to the width of grinding wheel because

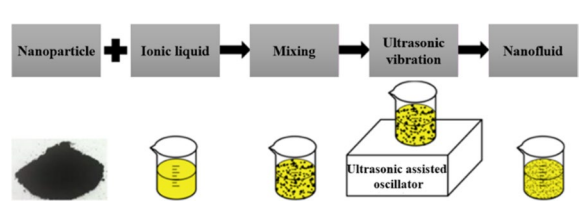

Figure 1 Preparation process of graphene/IL nanofluids

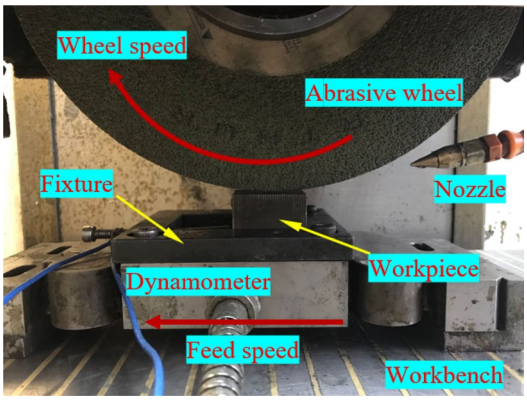

Figure 2 Grinding experimental platform

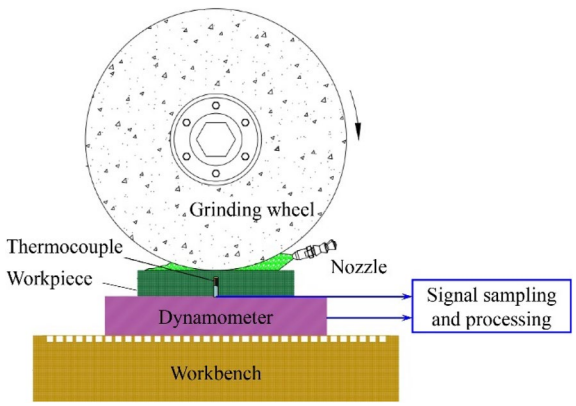

Figure 3 Grinding force and grinding temperature measurement scheme

of the greater workpiece width than the grinding wheel. Grinding force is measured by YDM- III99 three-phase dynamometer, and grinding temperature is measured by WRNK-191 thermocouple, as shown is shown in Figure 3. Before the beginning of each grinding experiment, the grinding wheel needs to be dressed. The specific grinding process parameters are shown in Table 2.

2.3 Measurement Schemes

Grinding force and grinding temperature are measured online. Grinding force is measured for 5–10 times under each group of parameters, and the measured values are averaged as the final result. The last measurement from the thermocouple before worn out is taken as grinding temperature measurement result, and the image of a worn-out thermocouple is shown in Figure 4. The VK-X1000 series shape measurement laser microscopic system is used to measure workpiece surface roughness, six positions are randomly selected for each workpiece, and the measured values are averaged as the final result.

Table 2 Grinding process parameters

Grinding parameters	Parameter setting
Grinding mode	Plane grinding
Grinding wheel	54A80F15VPH904W
Grinder	K-P36 surface grinder
Wheel speed (m/s)	30
Feed speed (mm/min)	600
Grinding depth (μm)	10, 20, 30
Grinding conditions	Dry, Flood, MQL, NMQL
Grinding fluids	Flood: water-solute liquid, 5% concentration MQL: [BMIM]BF_4, [HMIM]BF_4 NMQL: GN/BB, GN/HB nanofluids
Flood flow rate (L/h)	60
MQL/NMQL flow rate (mL/h)	50
MQL/NMQL gas pressure (MPa)	0.6
MQL/NMQL nozzle distance (mm)	17
MQL/NMQL nozzle angle (°)	15
Workpiece	GH4169, 40 mm × 30 mm × 30 mm
Dressing method	Single-point diamond dresser
Dressing depth (μm)	5
Dressing speed (mm/min)	600

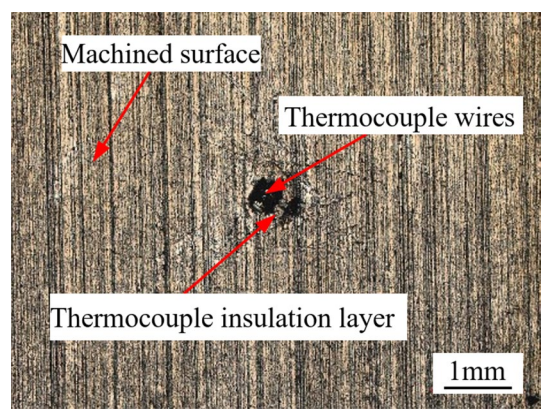

Figure 4 Microscopic images of a worn thermocouple

3 MQL Grinding Performances of Graphene/IL Nanofluids

Five parameters, i.e., specific grinding energy, grinding force ratio, surface roughness, grinding temperature and heat partition ratio, respectively, are used to quantitatively evaluate the MQL grinding performances of graphene/IL nanofluids.

3.1 Specific Grinding Energy

The specific grinding energy indicates the energy required to remove per unit volume of workpiece

material. This energy reflects the consumed energy of plasticity scratching and plowing in the grinding process, and it is an important index of grinding processing efficiency. The smaller grinding specific energy means the better lubrication effect in the grinding zone. The expression of specific grinding energy is shown in Eq. (1):

$$e_s = \frac{F_t \cdot v_s}{a_e \cdot v_w \cdot b}, \tag{1}$$

where F_t is the tangential grinding force, v_s is the grinding wheel peripheral speed, v_w is the workpiece feed speed, a_e is the grinding depth, and b is the grinding width.

The measured results of specific grinding energy under different cooling and lubricating conditions are shown in Figure 5. It can be seen that dry grinding obtains the largest values of specific energy, and this is inevitably in close relation with the lack of effective cooling and lubrication. And under the three grinding depths, NMQL conditions obtain lower values of specific energy compared with their corresponding MQL conditions.

At the grinding depth of 10 μm, NMQL conditions obtain much smaller values of specific grinding energy compared with flood and MQL conditions. In this condition, the GN/BB nanofluid obtains the minimum specific energy of 29.84 J/mm^3, and the GN/HB nanofluid is 38.53 J/mm^3. Compared with corresponding MQL grinding conditions that using [BMIM]BF_4 and [HMIM]BF_4 only, the GN/BB and GN/HB nanofluids can reduce specific grinding energy by 33.5% and 49.9%, respectively. And specific grinding energy is decreased by more than 55% compared with flood grinding. The results indicate that the two ILs and their corresponding nanofluids have better lubrication performance than flood lubrication.

When grinding depth increases to 20 μm, the specific grinding energy under NMQL is close to flood condition. MQL grinding with [BMIM]BF_4 obtains specific energy of 89.08 J/mm^3, and [HMIM]BF_4 obtains 91.28 J/mm^3. While under NMQL, the GN/BB and GN/HB nanofluids obtain values of 62.12 J/mm^3 and 71.45 J/mm^3, reduced by 30.3% and 21.7% compared with corresponding MQL conditions. With the increase of grinding depth, the grinding fluid entering the grinding zone decreases further, which makes the lubrication performance of the two ILs under the MQL condition is not as good as the flood lubrication. The addition of graphene enhances the lubrication performance of the ILs, ensuring that the lubrication effect is comparable to flood lubrication even the grinding fluid entering into the grinding zone is reduced.

At the grinding depth of 30 μm, the increase of grinding depth makes it more difficult for grinding fluid to enter into the grinding zone under MQL and NMQL conditions, which fails to achieve the desired lubrication effect. The flood lubrication flow is huge, and enough grinding fluid can enter into the grinding zone under the three grinding depths, so as to maintain good lubrication effect. The specific grinding energy under NMQL is slightly larger than that in flood grinding, however it is still smaller than that under MQL that using pure IL only.

3.2 Grinding Force Ratio

Grinding force ratio is the ratio between tangential force (F_t) and normal force (F_n). And the smaller grinding force ratio indicates the better lubrication effect in the grinding zone. The measured results of grinding force ratio are shown in Figure 6. It can be found that NMQL conditions

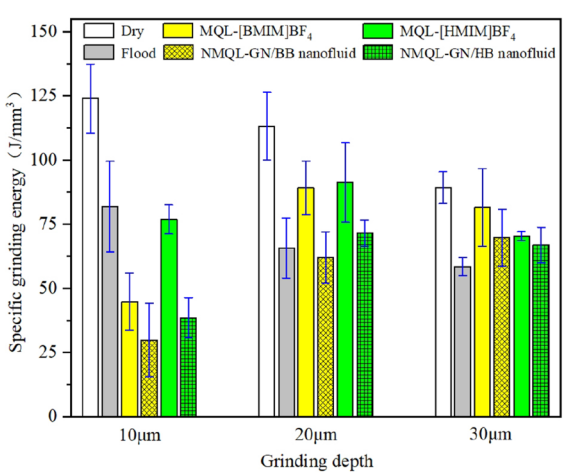

Figure 5 Measured results of specific grinding energy

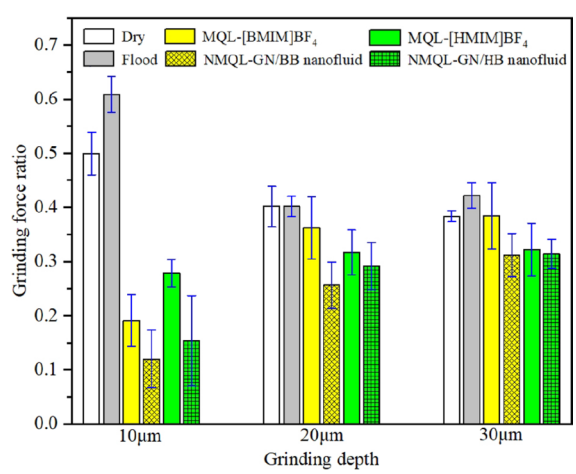

Figure 6 Measured results of grinding force ratio

obtain the least force ratios, and better lubrication effect can be obtained at smaller grinding depths.

At the grinding depth of 10 μm, the grinding force ratios of GN/BB and GN/HB nanofluids are 0.12 and 0.15, respectively, reduced by 42.1% and 46.4% compared with corresponding MQL conditions that using [BMIM]BF_4 and [HMIM]BF_4 only. Compared with flood grinding, grinding force ratios decrease by more than 75% under NMQL.

At the grinding depth of 20 μm, MQL grinding with [BMIM]BF_4 and [HMIM]BF_4 obtain force ratios of 0.36 and 0.32, respectively. Once graphene nanosheets are added, grinding force ratio can be further decreased. The GN/BB and GN/HB nanofluids obtain force ratios of 0.26 and 0.29, respectively, reduced by 16.7% and 9.4% compared with corresponding MQL conditions.

At the grinding depth up to 30 μm, although the wetting area decreases due to the increasing difficulty of nanofluid droplets entering into the grinding interface, grinding force ratios under NMQL are still smaller than those under flood and MQL grinding conditions.

3.3 Surface Roughness

Figure 7 displays the measured results of workpiece surface roughness at the grinding depth of 30 μm. It can be seen that the surface roughness in dry grinding is the largest, and the least surface roughness is obtained from the NMQL condition using GN/BB nanofluid. In this condition, the values of R_a and R_z obtained from GN/BB nanofluid are 0.7658 μm and 7.6808 μm, decreased by 16.3% and 16.1% compared with corresponding MQL condition that using [BMIM]BF_4 only. The values of R_a and R_z in NMQL grinding with GN/HB nanofluid are 0.8392 μm and 8.5308 μm, and they are reduced by 11.0% and 16.1% compared with corresponding MQL condition that using [HMIM]BF_4 only. Compared with flood grinding, both values of R_a and R_z under NMQL can be reduced by more than 20%.

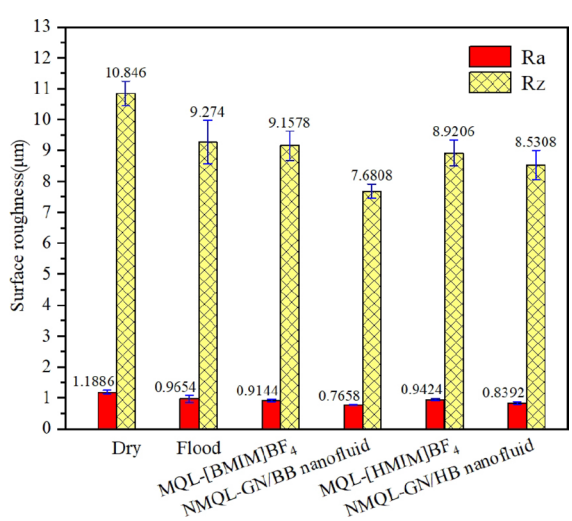

Figure 7 Measured results of surface roughness (a_e = 30 μm)

3.4 Grinding Temperature

Figure 8 displays the SEM pictures of workpiece machined surface morphology. It can be found that there is a very obvious grinding burn phenomenon in dry grinding, as shown in Figure 8(a). Whereas under flood (Figure 8(b)), MQL (Figure 8(c) and (d)) and NMQL (Figure 8(e) and (f)) conditions, grinding burn is hardly found. This indicates that both MQL and NMQL conditions can significantly reduce grinding temperature so as to avoid surface burn compared with dry grinding.

At the grinding depth of 30 μm, the measured results of grinding temperature under different conditions are shown in Figure 9. The measuring range of the thermocouples is no more than 415 °C. As the maximum temperature under dry grinding exceeds the range, the temperature curve under dry condition in Figure 9 is obtained from fitting the measured temperature signals within the measuring range. It can be seen that the fitted maximum grinding temperature is 426 °C. The measured maximum temperature under flood condition is 167.9 °C. In MQL grinding, the maximum temperatures obtained from [BMIM]BF_4 and [HMIM]BF_4 are 330.1 °C and

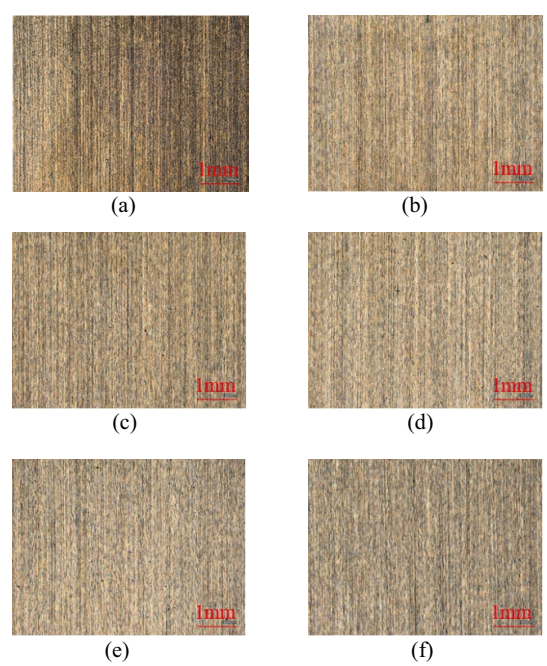

Figure 8 SME images of workpiece machined surface (a_e=30 μm): **a** Dry, **b** Flood, **c** MQL-[BMIM]BF_4, **d** NMQL-GN/BB nanofluid, **e** MQL-[HMIM]BF_4, **f** NMQL-GN/HB nanofluid

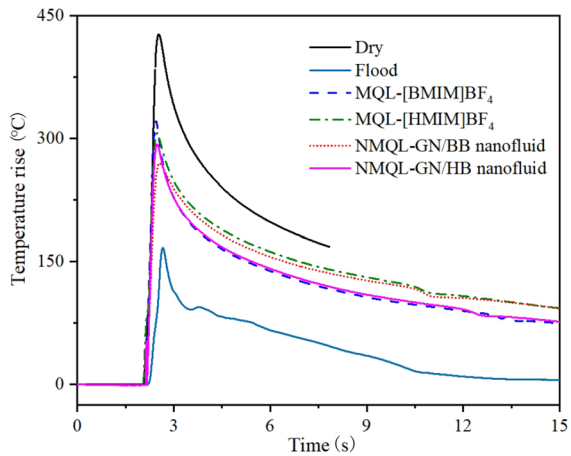

Figure 9 Measured results of grinding temperature (a_e = 30 μm)

321.1 °C, respectively, which are lowered about 100°C compared with dry grinding. In NMQL grinding, the maximum temperatures obtained from GN/BB and GN/HB nanofluids are 270.8 °C and 295.4 °C, respectively, which are further lowered by 18.0% and 8.0% compared with corresponding MQL grinding conditions. On one hand, this is because the addition of graphene nanosheets improves the tribological performance of MQL technology, thereby reducing the generation of grinding heat. On the other hand, graphene nanosheets enhance heat conduction (Table 3) and convective heat transfer in the grinding zone, thereby strengthening the heat transfer ability of MQL technology. The combined effect of the two aspects makes graphene/IL nanofluid further lower grinding temperature compared with using pure IL only.

3.5 Heat Partition Ratio

Heat partition ratio R_w is a critical parameter for thermal analysis of grinding, and it is defined as the ratio between the grinding heat transferred into the workpiece q_w and the total grinding heat q, which can be expressed as $R_w = q_w/q$. The smaller heat partition ratio is, the less heat will be transferred into the workpiece, and the better cooling performance under this condition. The total grinding heat q and the heat transferred into the workpiece q_w can be calculated from Eqs. (2) and (3) [43]:

$$q = \frac{F_t v_s}{b l_c}, \tag{2}$$

$$q_w = \frac{k_w v_w^{1/2}}{\beta \alpha_w^{1/2} l_c^{1/2}} T_{max}, \tag{3}$$

where l_c is the length of grinding zone, and can be obtained from $l_c = (a_e d_s)^{1/2}$, d_s is the diameter of grinding wheel, k_w is the workpiece thermal conductivity, β indicates a constant and its value depends on the heat source profile, for triangular heat source its value is 1.06, α_w is the thermal diffusivity of workpiece, and can be calculated from $\alpha_w=(k_w \rho_w c_w)^{1/2}$, ρ_w and c_w are density and specific heat capacity, for GH 4169 their values are 8.24 g/m^3 and 451.2 J/(kg·°C), obtained from Ref. [44], T_{max} is the workpiece maximum temperature rise, and can be calculated from $T_{max}=T_m-T_{in}$, and

T_m is the measured maximum grinding temperature,

T_{in} is the ambient temperature.

The measured results of heat partition ratio are shown in Figure 10. It can be seen that flood grinding obtains the minimum heat partition ratio of 0.36, and the maximum heat partition ratio of 0.58 is obtained in dry grinding. In general, the heat partition ratio in dry grinding is more than 0.7 when corundum grinding wheel is used. This indicates that the fitted maximum grinding temperature in dry grinding, i.e., 426 °C, should be lower than the actual condition. In MQL grinding, the heat partition ratios from [BMIM]BF$_4$ and [HMIM]BF$_4$ are 0.51 and 0.57. Under NMQL, the heat partition ratios from GN/BB and GN/HB nanofluids are 0.49 and 0.55, lowered by

Table 3 Thermal conductivity of ILs and graphene/IL nanofluids

Grinding fluid	Thermal conductivity at 25 °C (W/(m·K))
[BMIM]BF$_4$	0.163
[HMIM]BF$_4$	0.170
GN/BB nanofluid	0.217
GN/HB nanofluid	0.214

Measured by TC3000E thermal conductivity instrument

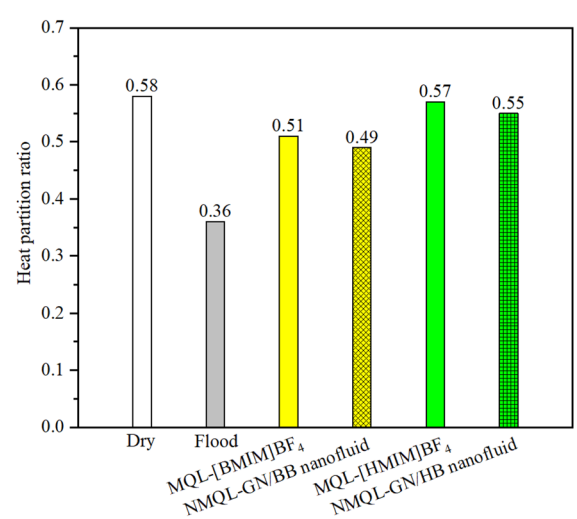

Figure 10 Results of heat partition ratio (a_e = 30 μm)

3.9% and 3.5% compared with corresponding MQL conditions. However, in the case of flood grinding, the heat partition ratio is only 0.36. This indicates that the heat transfer ability of NMQL technique is still insufficient compared with conventional flood grinding.

It can be ascertained that the cooling effect of NMQL is indeed better than that of MQL, however its heat transfer ability is not reaching ideal status compared with flood grinding. This is mainly because the droplet flow rate entering into the grinding zone is too little, which hardly achieves the level in flood grinding. The reason for that the addition of graphene nanosheets into ILs can further lower grinding temperature, mainly depends on the improvement of tribological properties of base fluids, thus lowering the heat generation in the grinding zone.

In summary, under the condition at shallow grinding depth, better lubrication performance can be obtained in MQL grinding that using IL only, compared with flood grinding. As grinding depth increases, it is more difficult for spray droplets to enter into abrasive grain/workpiece grinding interface, resulting in the insufficient lubrication performance. Once graphene nanosheets are introduced, the values of the five parameters can be further reduced. In short, graphene/IL nanofluid can strengthen both the cooling and lubricating performance of the MQL technique that using IL only.

4 Formation Mechanism of Lubrication Film on Grain/Workpiece Grinding Interface under NMQL with Graphene/IL Nanofluid

The evaluation of MQL grinding performance shows that NMQL grinding with graphene/IL nanofluids not only can strengthen the heat transfer ability of MQL technique, but also can further improve the tribological performances of friction reducing and anti-wear. This indicates that the introduction of graphene nanosheets make changes to the formation mechanism of the lubrication film on abrasive grain/workpiece grinding interface. This section firstly performs molecular dynamics simulations of abrasive grain/workpiece interface to explore the formation mechanism of physical adsorption film resulting from graphene/IL nanofluid. Afterwards, EDS and XPS analyses of workpiece machined surface are carried out to explore the formation mechanism of chemical reaction film.

4.1 Molecular Dynamics Simulation of Abrasive Grain/Workpiece Grinding Interface

Molecular dynamics simulations are performed in LAMMPS, and are visualized in OVITO. The establishment scheme of molecular dynamics model is shown in Figure 11. In addition to NQML condition that using graphene/IL nanofluid, the simulation under MQL condition

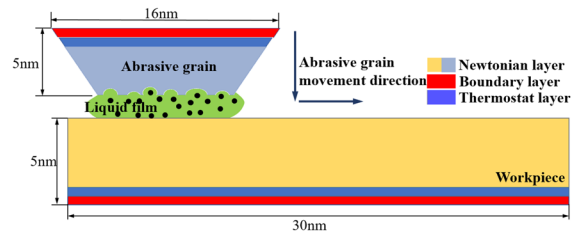

Figure 11 Molecular dynamics model

that using [BMIM]BF_4 only is also performed to act as control group for subsequent comparative analyses.

4.1.1 Geometric Models

Single crystal Ni-Fe-Cr series of Ni-based alloy is used as workpiece material which possesses face-centered cubic (FCC) structure with lattice constant of 0.352 nm [45]. The element composition and content of the workpiece are shown in Table 4. In order to simplify the model, the portions of Ni, Fe and Cr atoms are set to be 52%, 30% and 18%, respectively. The workpiece is modeled as the cuboid shape with the size of 30 nm× 11 nm× 5 nm, and it is successively divided into boundary, thermostat and newton layers along the positive direction of z axis, as shown in Figure 12. The thicknesses of boundary and thermostat layers both are set to be 0.5 nm.

The abrasive grain material is single crystal Al_2O_3 with corundum lattice structure. The Al_2O_3 grain is modeled to be the quadrangular frustum pyramid shape. The side length of the top face is 16 nm, and the height is 4 nm, as shown in Figure 13(a). Its side faces are modeled to be uneven, and its wear flat face is modeled with groove-like fractures. This modeling is consistent with the actual status of the abrasive grains on the surface of ceramic white corundum grinding wheel, as shown in Figure 13(b). The abrasive grain model is also divided into boundary, thermostat and newton layers along the negative direction of z axis. And the boundary and thermostat layers also both are 0.5 nm in thickness.

The establishment of [BMIM]BF_4 liquid film can also be found in the previous research [42]. There is total 380 [BMIM]BF_4 molecules to form ionic liquid film, randomly distributed in an 10 nm × 10 nm × 2 nm simulation box, as shown in Figure 14(a). The ionic liquid film is divided into thermostat and newton layers. The thermostat layer is set to be a square shape with side length of 1 nm, and it is located in the center of the ionic liquid film, as shown in Figure 14(b). The rest atoms all belong to the newton layer.

The establishment of GN/BB nanofluid film needs to obtain the models of graphene nanosheet and [BMIM] BF_4 molecule firstly. The optimal configuration of

Table 4 Element composition and content [46]

Element	Ni	Cr	Mo	Si	Mn	Co
Content	50–55	17–21	2.8–3.3	0.35	0.35	1.0
Element	Al	Nb	Fe	S	C	Cu
Content	0.2–0.8	4.7–5.5	remainder	0.01	0.08	0.3

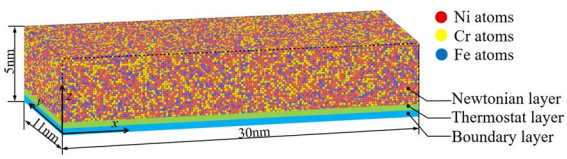

Figure 12 Workpiece model

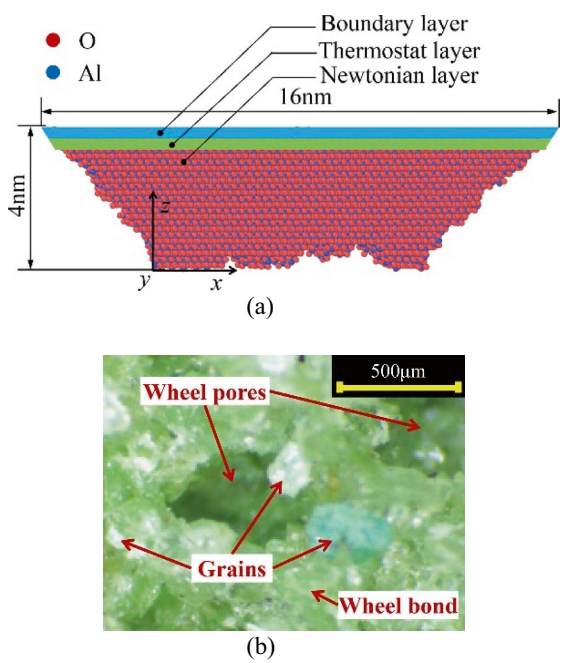

Figure 13 Establishment of abrasive grain model: **a** Abrasive grain model, **b** Optical microscope image of grinding wheel surface

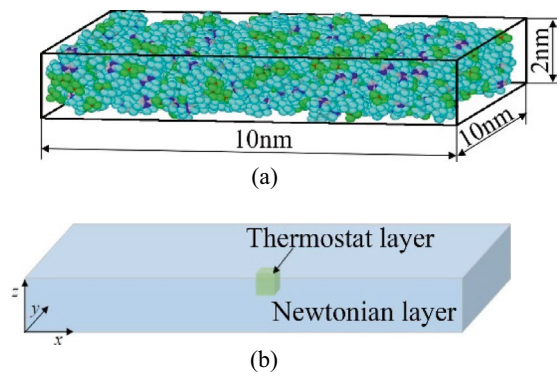

Figure 14 Establishment of ionic liquid film model: **a** [BMIM]BF_4 liquid film, **b** Thermostat layer setting

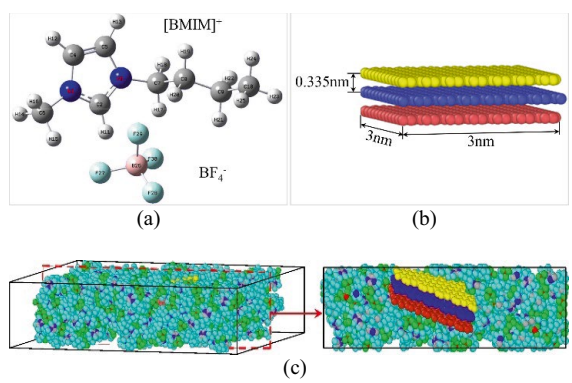

Figure 15 Establishment of GN/BB nanofluid film model: **a** [BMIM] BF_4 molecule model, **b** Trilayer graphene model, **c** GN/BB nanofluid film

[BMIM]BF_4 molecule has been acquired in the previous research [41], as shown in Figure 15(a). The ABA-stacked trilayer graphene is modeled in LAMMPS. Its length and width are both 3nm, and its interlayer spacing is 0.335 nm, as shown in Figure 15(b). Afterwards, the trilayer graphene and 380 [BMIM]BF_4 molecules are randomly mixed in an 10 nm × 10 nm × 2 nm simulation box to form GN/BB nanofluid film, as shown in Figure 15(c). The nanofluid film is also divided into thermostat and newton layers, using the same setting method as ionic liquid film.

4.1.2 Simulation Details

During molecular dynamics simulations, the length and height directions of the workpiece are both set as fixed boundary conditions, and the width direction is set as periodic boundary condition. Each simulation can be divided into the relaxation, descent and grinding stages, and the time steps in each stage are all 1 fs. The simulation details in each stage are almost the same as the previous research [42], except the following settings. In

the descent stage, the depth of abrasive grain penetrating into the workpiece is 2 nm. And in the grinding stage, the total grinding distance of abrasive grain is 10 nm.

4.1.3 Potential Functions

The interactions of atoms in Al_2O_3 grain, workpiece, and IL can be described with Vashishta potential function [47], EAM potential function [48] and all-atom force field [49], respectively. The interactions of atoms between abrasive grain and workpiece can be described with Morse potential function, which is expressed with Eq. (4):

$$E = D_0[e^{-2\alpha(r-r_0)} - 2e^{-\alpha(r-r_0)}], \tag{4}$$

where D_0 and α scale the strength and scope of the interaction, respectively, r_0 is the atomic equilibrium distance. The Morse potential parameters are listed in Table 5.

The interactions of atoms in the trilayer graphene include intra- and inter-layer interactions. The intra-layer interactions can be described with the Tersoff potential function [51], which has been integrated into LAMMPS and can be invoked directly. The inter-layer interactions can be described with Lennard-Jones potential function, which is expressed with Eq. (5):

$$E(r_{ij}) = 4\varepsilon_{ij}\left[\left(\frac{\sigma_{ij}}{r_{ij}}\right)^{12} - \left(\frac{\sigma_{ij}}{r_{ij}}\right)^{6}\right], \tag{5}$$

where σ_{ij} is the distance parameter that represents the equilibrium distance between atoms i and j, ε_{ij} is the energy parameter, and r_{ij} is the distance between the two interacting atoms. For the inter-layer C–C interactions, the values of ε and σ are set to be 2.964 meV and 3.407 Å, respectively, and the cutoff radius is set to be 10 Å [52].

Besides the interactions within graphene sheet and IL, the interactions of atoms in the nanofluid film also include the interactions between them, which can also be described with Lennard-Jones potential function. The Lennard-Jones potential parameters are listed in Table 6, obtained from the UFF force field model in Ref. [53]. And the cutoff radius of these Lennard-Jones interactions is set to be 15 Å.

Table 5 Morse potential parameters [50]

Workpiece	Abrasive grain	D_0 (eV)	α (1/Å)	r_0 (Å)
Ni	Al	0.33713	1.2924	2.8083
	O	0.475	1.398	3.238
	Al	0.33589	1.2767	2.8376
Fe	O	0.473	1.382	3.275
Cr	Al	0.34541	1.3685	2.8199
	O	0.487	1.474	3.698

Table 6 Lennard-Jones parameters for interactions between graphene sheet and ionic liquid

Graphene	Ionic liquid	ε (eV)	σ (Å)
C	N	0.003691	3.3458
	C	0.0045532	3.4309
	H	0.0029475	3.001
	B	0.0059616	3.5342
	F	0.003142	3.2139

The interactions of atoms between nanofluid film and abrasive grain, and between nanofluid film and workpiece, can also be described with Lennard-Jones potential function. And the Lennard-Jones potential parameters are listed in Table 7, also obtained from the UFF force

Table 7 Lennard-Jones parameters for interactions between nanofluid film and the rest atoms

Nanofluid film		Workpiece	Grain	ε (eV)	σ (Å)
Ionic liquid	N		Al	0.008095	3.6344
			O	0.00279	3.1894
		Ni		0.001395	2.8927
		Fe		0.001395	2.9769
		Cr		0.001299	2.9275
	C		Al	0.009986	3.7195
			O	0.003442	3.2745
		Ni		0.001721	2.9778
		Fe		0.001721	3.062
		Cr		0.001602	3.0126
	H		Al	0.006464	3.2896
			O	0.002228	2.8446
		Ni		0.001114	2.548
		Fe		0.001114	2.6322
		Cr		0.001037	2.5827
	B		Al	0.013074	3.8228
			O	0.004507	3.3778
		Ni		0.002253	3.0812
		Fe		0.002253	3.1654
		Cr		0.002098	3.1159
	F		Al	0.006891	3.5026
			O	0.002375	3.0576
		Ni		0.001188	2.7609
		Fe		0.001188	2.8451
		Cr		0.001106	2.7956
Graphene	C		Al	0.009986	3.7195
			O	0.003442	3.2745
		Ni		0.001721	2.9778
		Fe		0.001721	3.062
		Cr		0.001602	3.0126

field model in Ref. [53]. The cutoff radius of all these interactions also is set to be 15 Å.

4.1.4 Results and Discussions

(1) Grinding Force and Grinding Force Ratio

Under NMQL using graphene/IL nanofluid, the contact states on the abrasive grain/workpiece grinding interface at different grinding distances are provided in Figure 16. It can be found that the whole grinding process can be divided into the following two grinding stages: I and II. In grinding stage I, the interlayer shear effect of the trilayer graphene occurs within the grinding distance of 4.7 nm, as shown in Figure 16(a). In grinding stage II, the interlayer shear effect is over, corresponding to the residual grinding stroke of the abrasive grain, as shown in Figure 16(b).

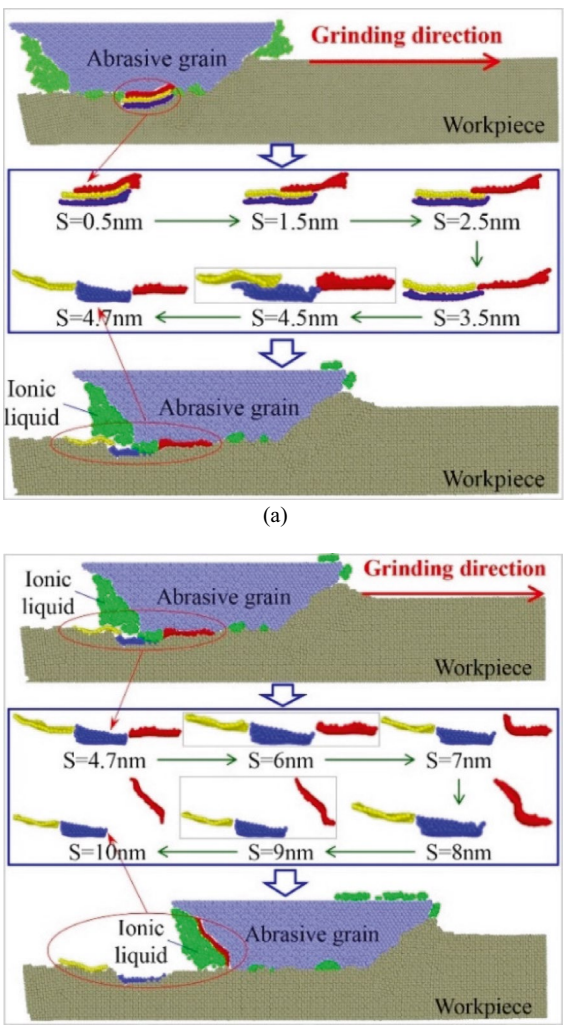

Figure 16 The contact states on abrasive grain/workpiece grinding interface: **a** Stage I: interlayer shear effect occurs, **b** Stage II: interlayer shear effect ends

In the two grinding stages above, the calculated results of tangential grinding force and grinding force ratio under MQL and NMQL conditions are shown in Figure 17. It can be discovered from Figure 17(a) and (b) that during stage I with the occurrence of interlayer shear effect, the average tangential force in NMQL grinding is 268.14 nN, and is reduced by 10.8% compared with MQL grinding. During stage II that the interlayer shear effect is over, the average tangential force in NMQL grinding is 296.69 nN, and this value is very close to that in MQL grinding. However, the average tangential force in NMQL grinding during stage II is 10.6% larger than that during stage I. This indicates that the interlayer shear effect of graphene nanosheets is closely related to the reduction of tangential grinding force. From Figure 17(c) and (d), it can be found that the interlayer shear effect also has an important influence on grinding force ratio. During stage I in NMQL grinding, the force ratio is 0.3794, while it is 0.3952 during stage II, 4.2% larger than that in stage I. During stage I with the occurrence of interlayer shear effect, the grinding force ratio under NMQL condition decreases about 1.6% compared with MQL condition. The experimental results in Figure 6 also show that the grinding force ratio under NMQL condition decreases somewhat compared with MQL condition. This indicates that the graphene nanosheets can successfully enter into the grinding interface and can provide good lubrication performance. The simulations obtain similar qualitative laws with experimental results, which can be concluded that graphene nanosheets utilize its interlayer shear effect to enhance the lubricating performance of the MQL technique.

As pointed in the previous research [42], [BMIM]BF_4 molecules absorb in the groove-like fractures on grain wear flat face to form boundary lubrication film between abrasive grain and workpiece, as shown in Figure 18(a). As the introduction of graphene nanosheet, it can enter into abrasive grain/workpiece grinding interface so as to reduce the contact area between the abrasive grain and the workpiece, as shown in Figure 18(b). In this condition, the friction force between the abrasive grain and the workpiece can be expressed as

$$F_f = \tau_s A_s + \tau_{gn} A_{gn} + \tau_l A_l, \tag{6}$$

where τ_s is the shear strength of workpiece material, A_s is the contact area between abrasive grain and workpiece, τ_{gn} is the interlayer shear strength of graphene, A_{gn} is the action area of graphene, τ_l is the viscous resistance of IL, A_l is the action area of lubricating film. Compared with MQL grinding using IL only, NMQL grinding with

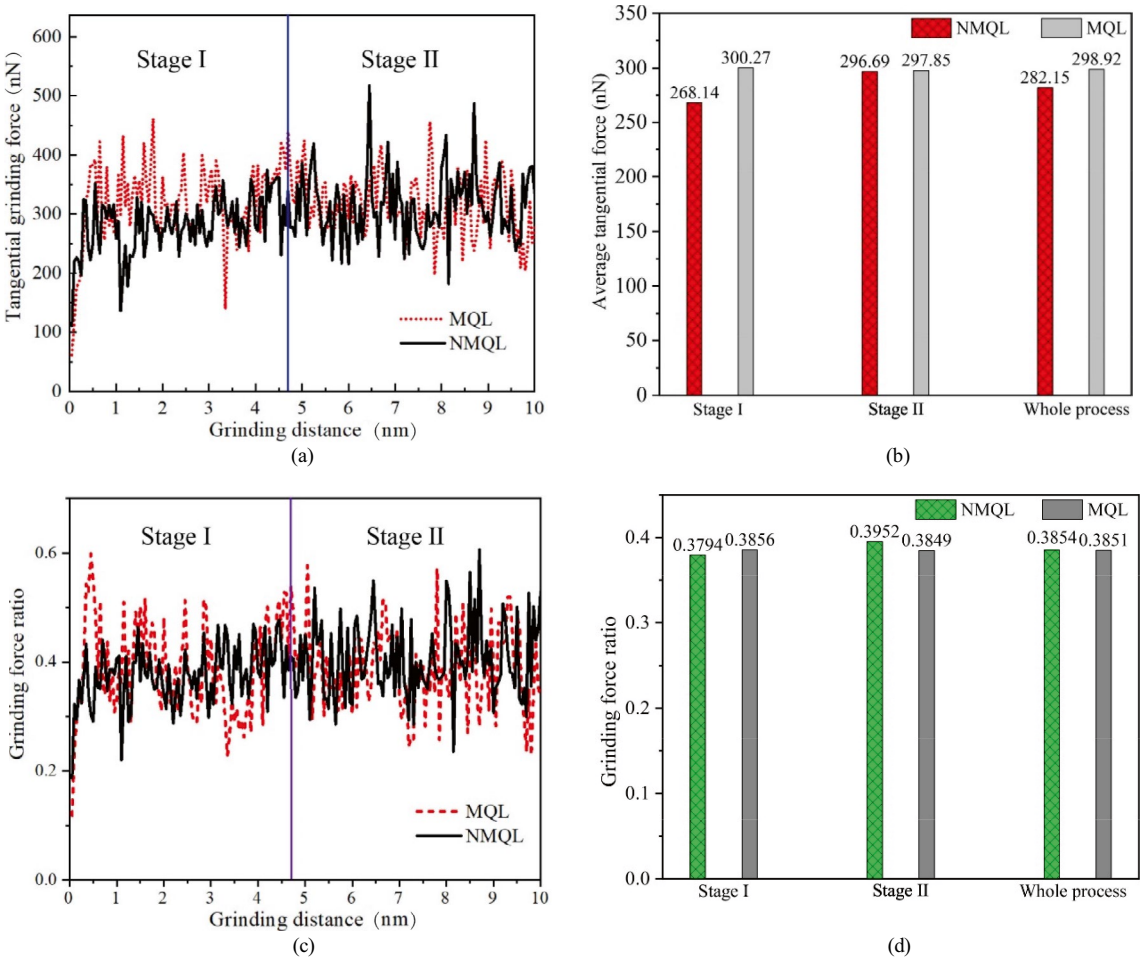

Figure 17 Calculations of tangential grinding force and grinding force ratio: **a** Evolution of tangential grinding force, **b** Average tangential grinding force, **c** Evolution of grinding force ratio, **d** Average grinding force ratio

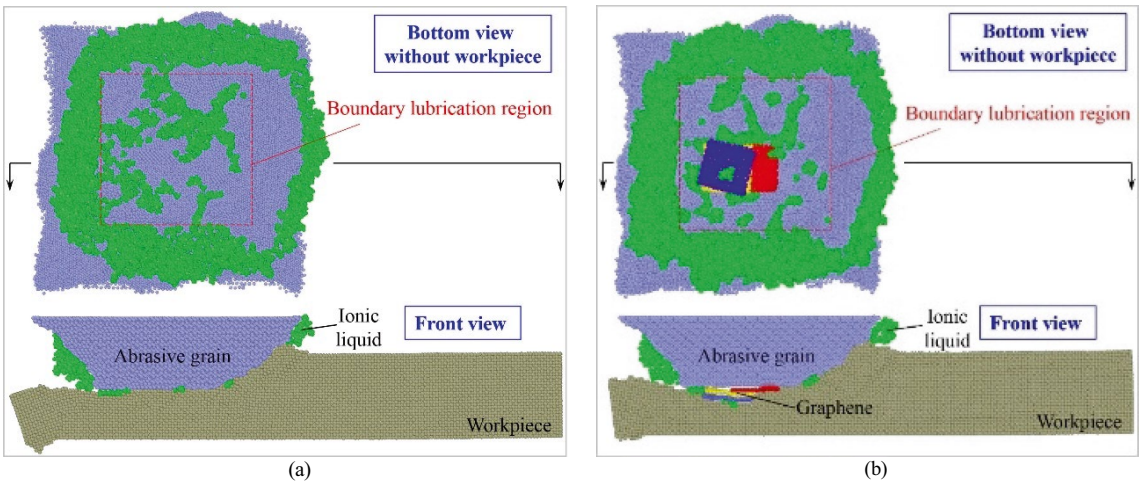

Figure 18 The boundary lubrication status on the abrasive grain/workpiece grinding interface: **a** MQL grinding, **b** NMQL grinding

graphene/IL nanofluid can reduce the contact area A_s, and the reduced area is just equal to the action area of graphene A_{gn}. The interlayer shear strength of graphene is much lower than the shear strength of workpiece material, and this mainly induces the reduction of tangential grinding force in NMQL grinding.

Although there are some discrepancies between the experimental and the simulated results of grinding force and grinding force ratio, similar qualitative law can be obtained that the interlayer shear effect of graphene can further strengthen the tribological performance on abrasive grain/workpiece grinding interface. This can also prove the correctness of the molecular dynamic simulations.

(2) Grinding Temperature

Figure 19 depicts the grinding temperature distributions under MQL and NMQL conditions, where Figure 19(a) and (b) are at grinding distance of 1.5 nm that the interlayer shear effect occurs, and Figure 19(c) and (d) are at grinding distance of 6 nm that the interlayer shear effect is over. It can be discovered that high temperature region is mainly located near the cutting edge of abrasive grain. At the grinding distance of 1.5 nm, the area of high temperature region under NMQL is reduced clearly compared with MQL. However, at the grinding distance of 6 nm, the area under NMQL is only slightly reduced. This indicates once again that the enhancement of lubricating performance induced by the interlayer shear effect has an important influence on lowering grinding temperature.

(3) Lattice Structure Evolution

Grinding force and grinding heat fundamentally result from the evolution of initial FCC lattice structure of workpiece material transformed into other lattice structures under the jostling action of abrasive grain, leading to the nucleation and propagation of dislocations. Therefore, the evolution of internal lattice structure of workpiece is analyzed with the PTM method, as shown in Figure 20, so as to revel the effect mechanism of graphene nanosheet on reducing grinding force and grinding temperature.

The initial lattice structure of workpiece material is FCC structure, and the action of external force induces the occurrence of lattice deformation, lattice

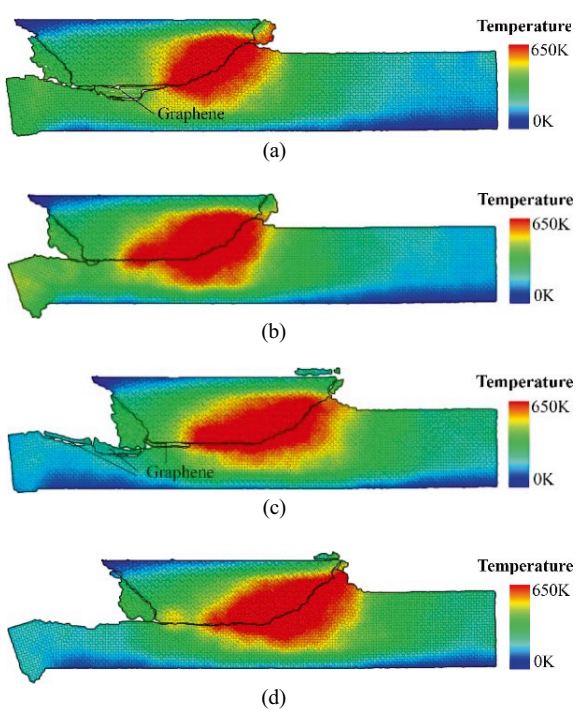

Figure 19 Grinding temperature distributions: **a** NMQL grinding at the distance of 1.5 nm, **b** MQL grinding at the distance of 1.5 nm, **c** NMQL grinding at the distance of 6 nm, **d** MQL grinding at the distance of 6 nm

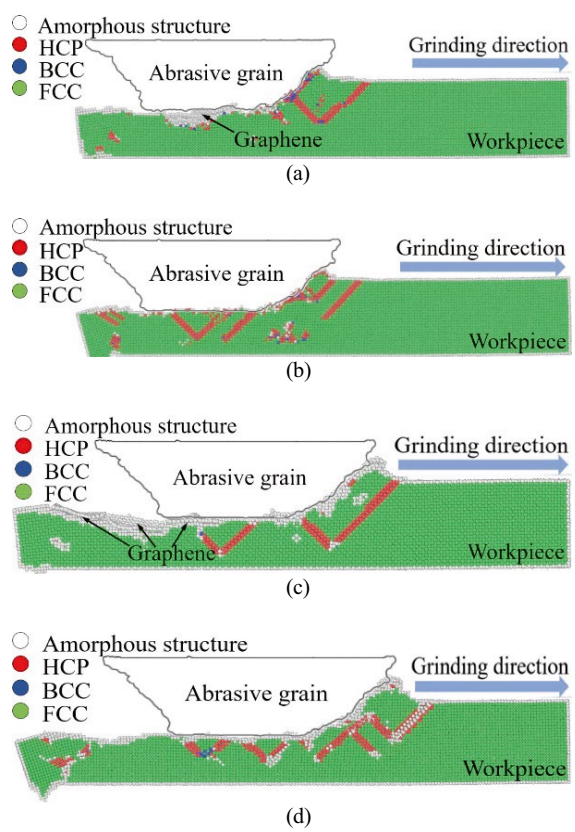

Figure 20 The internal lattice structures of workpiece: **a** NMQL grinding at the distance of 1.5 nm, **b** MQL grinding at the distance of 1.5 nm, **c** NMQL grinding at the distance of 6 nm, **d** MQL grinding at the distance of 6 nm

reconfiguration and amorphous phase transition inside the workpiece during the grinding process. The variations of lattice structures lead to the fluctuations of grinding force and the distribution of grinding temperature. During the grinding process, the abrasive grain jostles workpiece material and obliges orderly arranged workpiece atoms to be disordered. This causes the initial FCC lattice structure mostly transformed into amorphous and HCP structures, and a small part transformed into BCC structure. The phase transformations of internal lattice structure are mainly generated underneath grain wear flat face and ahead of grain cutting edge, as shown in Figure 20. The amorphous structures will mostly be transformed into other lattice structures as the grinding process continues, and a small part will be removed along with grinding chips.

At the grinding distance of 1.5 nm that the interlayer shear effect of graphene occurs, the lattice structures of the workpiece under NMQL and MQL conditions are provided in Figure 20(a) and (b). It can be observed that the HCP lattice structure under NMQL is much less than MQL, especially underneath the abrasive grain where the graphene nanosheet exists, these phase transformations are generated mainly by the jostling action of abrasive grain. During the phase transformation, the atomic strain of workpiece material increases continuously, and once the atomic strain exceeds the threshold of thermodynamic phase transformation, the atoms of workpiece will be in a quasi-stable state. As the atomic strain increases continuously, the initial FCC lattice structure will be in a state of absolute instability, and can lead to the mutations of mechanical quantities. In order to relax lattice strain, dislocations will nucleate and propagate to release partial strain energy, causing the fluctuation of grinding force and the generation of grinding heat. From Figure 20(a) and (b), it can be obtained that the interlayer shear effect of graphene can reduce the external force acting on the workpiece from the abrasive grain, so as to maintain the relative stability of workpiece atoms, resulting in lowering grinding force and grinding heat.

Figure 20(c) and (d) show the lattice structure distributions inside the workpiece at the grinding distance of 6 nm that the interlayer shear effect is over. It can be found that HCP structure is generated underneath the abrasive grain in NMQL grinding, whereas they are not appeared at the grinding distance of 1.5 nm. This once again ascertains the important influence of the interlayer shear effect on reducing grinding force between abrasive grain and workpiece.

From the molecular dynamics simulations, it can be concluded that boundary lubrication film is also formed on abrasive grain/workpiece interface in NMQL grinding with graphene/IL nanofluid. Besides IL molecules absorbing in the groove-like fractures on grain wear flat face, graphene nanosheet can enter into the interface between abrasive grain and workpiece to decrease their contact area. Benefitting from the interlayer shear effect of graphene and its much lower interlayer shear strength than workpiece material, the lubricating performance on abrasive grain/workpiece grinding interface can be further enhanced, resulting in lower grinding force, grinding heat, and thus grinding temperature, compared with MQL grinding using IL only.

4.2 EDS and XPS Analyses of Workpiece Machined Surfaces

The formation mechanism of physical adsorption film resulted from graphene/IL nanofluid has already been revealed through molecular dynamics simulation. This section will perform EDS and XPS analyses of workpiece machined surfaces to research the distribution and valence states of chemical elements, so as to explore the formation mechanism of chemical reaction film on abrasive grain/workpiece grinding interface under NMQL with graphene/IL nanofluid.

The Zeiss Merlin field emission scanning electron microscope (FE-SEM) attached with energy dispersive X-ray spectroscopy (EDS) system is used to perform SEM and EDS analyses, so as to analyze the distribution of chemical elements. The PHI5000 Versaprobe III X-ray photoelectron spectroscopy (XPS) analyzer is used to analyze the valence states of chemical elements. Before the analyses, all the specimens are immersed in alcohol and subsequently cleaned by ultrasonic oscillator. For each specimen, each analysis will be performed at least three detecting positions.

4.2.1 Distribution of Chemical Elements on Workpiece Machined Surface

The results of EDS analyses of workpiece machined surfaces in NMQL grinding are presented in Figure 21. It can be discovered from the SEM images that dark gray patches exist on the machined surfaces, of which the sizes are equivalent to the diameter (1–3 μm) of graphene nanosheets used in grinding experiments. Further EDS analyses indicate that carbon elements gather within the patches in high density. Therefore, it can be determined that the dark gray patches are graphene nanosheets. This clearly indicates that graphene nanosheets can enter into abrasive grain/workpiece grinding interface successfully, and can be 'welded' on the workpiece machined surface under the actions of high temperature and high pressure. This phenomenon can also be obtained from the molecular dynamics simulations, as shown in Figure 22.

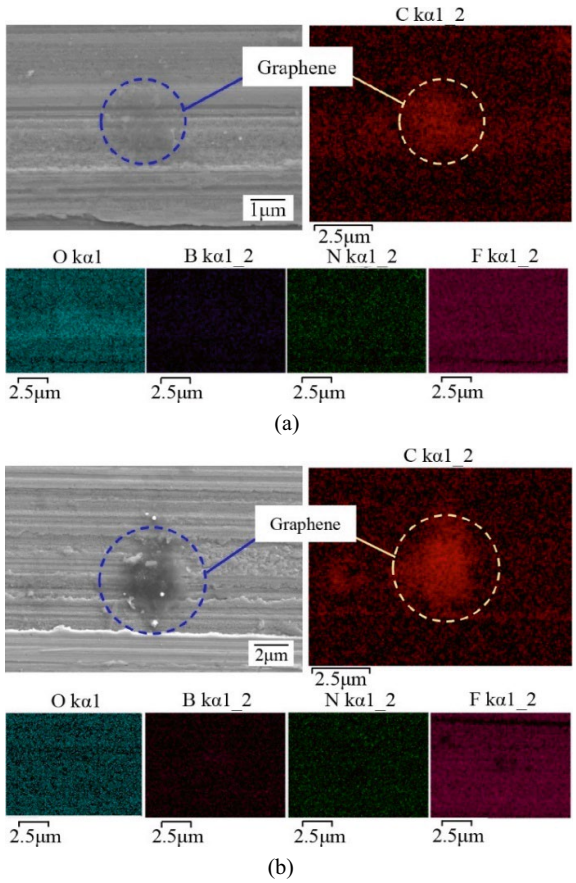

Figure 21 The results of EDS analyses of workpiece machined surfaces in NMQL grinding: **a** GN/BB nanofluid, **b** GN/HB nanofluid

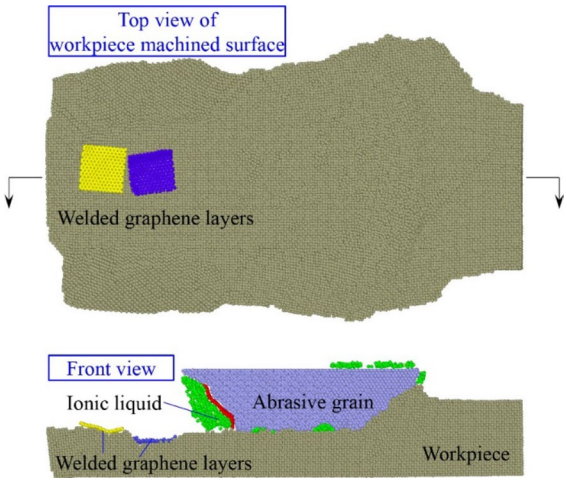

Figure 22 Phenomenon of welded graphene layers from molecular dynamics simulation

It can also be found from Figure 21 that those chemical elements such as O, B, N, and F, are detected on workpiece machined surface, however those elements are not contained in workpiece material. Therefore, it can be reasonably speculated that workpiece material happens chemical reactions with graphene/IL nanofluids during NMQL grinding, producing fluorides and nitrides. The oxides should be produced by air oxidation of workpiece machined surface. In the following research, XPS analyses of workpiece machined surfaces are further carried out to validate this speculation.

4.2.2 Valence States of Chemical Elements on Workpiece Machined Surface

The results of XPS analyses in NMQL grinding with GN/BB nanofluid are provided in Figure 23. The binding energy peaks of Ni 2p appear at 854.7 eV and 872.7 eV, and both are ascribed to NiO. Two obvious binding energy peaks of Fe 2p locate at 709.9 eV and 711.4 eV, corresponding to Fe_2O_3 and FeF_2, respectively. One of Cr 2p binding energy peaks at 579.8 eV is assigned to CrF_3, and the other two peaks at 579.8 eV and 587.1 eV are both attributed to Cr_2O_3. Two binding energy peaks of F 1s at 684.9 eV and 685.5 eV belong to FeF_2 and CrF_3, respectively. The binding energy peaks of N 1s and B 1s are 191.0 eV and 398.6 eV, and both are corresponding to BN. From the XPS analyses above, it can be concluded that during NMQL grinding with GN/BB nanofluid, the negative and positive ions of $[BMIM]BF_4$ will decompose

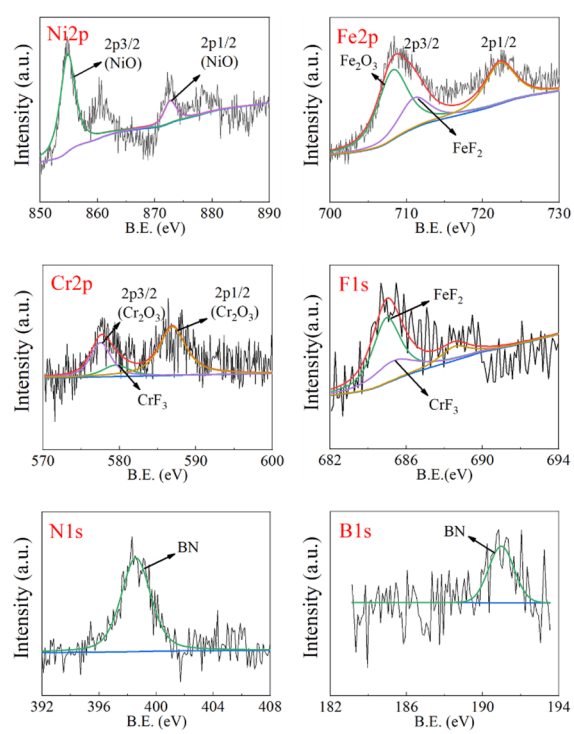

Figure 23 XPS spectra of workpiece machined surface in NMQL grinding with GN/BB nanofluid

under the actions of high temperature and high pressure, and react with workpiece material, producing fluorides and nitrides, such as FeF_2, CrF_3, and BN. The metallic oxides, such as NiO, Fe_2O_3 and Cr_2O_3, are produced by air oxidation due to the high chemical activity of fresh machined surface of workpiece.

The XPS spectra of workpiece machined surface using GN/HB nanofluid are depicted in Figure 24. It can be discovered that Ni element exists in the form of NiO, and B and N elements exist together in BN. For Cr and Fe elements, they exist not only in their respective oxides of Cr_2O_3 and Fe_2O_3, but also in fluorides of CrF_3 and FeF_2. Therefore, it can be concluded that $[HMIM]BF_4$ also happens chemical reactions with workpiece material, and thus FeF_2, CrF_3, and BN are produced. The metallic oxides are also produced by air oxidation of fresh machined surface of workpiece.

From the EDS and XPS analyses above, it can be summarized that only IL base fluid happens chemical reactions with workpiece material in NMQL grinding with graphene/IL nanofluid. Graphene nanosheets are not involved in chemical reactions, and can be 'welded' on workpiece machined surface by physical adsorption, playing a role in filling and repairing the machined surface, so as to reduce the surface roughness of the machined surface. The chemical reactions between IL and workpiece material can produce fluorides and nitrides, and metallic oxides can also be produced by air oxidation of fresh machined surface. These fluorides, nitrides and oxides together constitute chemical reaction film with low shear strength and excellent friction-reducing and anti-wear properties [54–56].

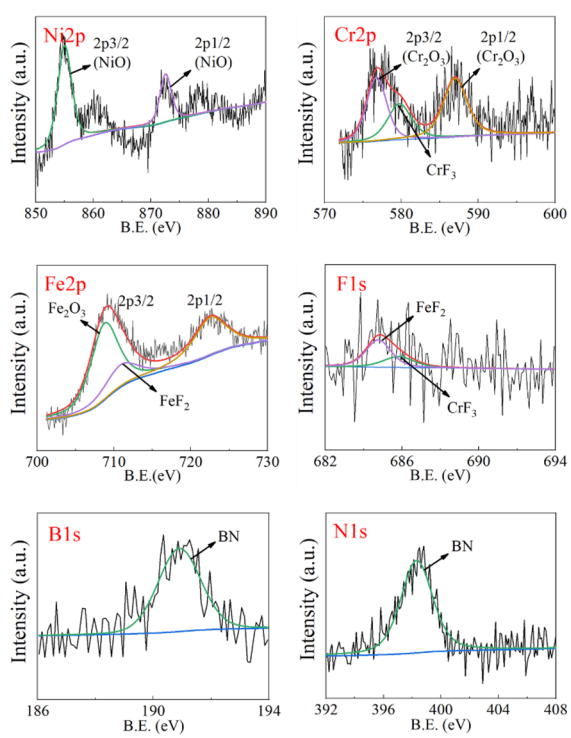

Figure 24 XPS spectra of workpiece machined surface in NMQL grinding with GN/HB nanofluid

5 Conclusions

(1) Compared with MQL grinding using ionic liquid (IL) only, NMQL grinding with graphene/IL nanofluid can further strengthen both the cooling and lubricating performances. In terms of lubrication, graphene/IL nanofluid can reduce specific grinding energy and grinding force ratio by over 40% at grinding depth of 10 μm, and can lower surface roughness by over 10% at grinding depth of 30 μm, compared with using IL only. In terms of cooling, graphene/IL nanofluid can lower grinding temperature over 50 ℃ at grinding depth of 30 μm, compared with using pure IL only. However, the heat transfer ability of NMQL is still insufficient compared with flood grinding.

(2) Abrasive grain/workpiece grinding interface is in a boundary lubrication state under NMQL with graphene/IL nanofluid. On one hand, IL molecules absorb in groove-like fractures on grain wear flat face to form boundary lubrication film. On the other hand, graphene nanosheets can enter into the grinding interface to further decrease the contact area between abrasive grain and workpiece. The interlayer shear effect and low interlayer shear strength of graphene nanosheets can further enhance the lubricating performance on the grinding interface, resulting in lower grinding force, grinding heat and thus grinding temperature, compared with MQL using IL only.

(3) Chemical reactions between base fluid and workpiece material happen in NMQL grinding with graphene/IL nanofluid, by which fluorides and nitrides can be produced, such as FeF_2, CrF_3, and BN. Metallic oxides, such as NiO, Cr_2O_3 and Fe_2O_3, can also be produced by air oxidation of fresh machined surface of workpiece. The fluorides, nitrides and oxides together constitute chemical reaction film, possessing low shear strength and excellent friction-reducing and anti-wear properties. Graphene nanosheets are not involved in the chemical reactions during the grinding process.

Acknowledgements
Not applicable.

Authors' Contributions
DW and YZ wrote the manuscript; QZ assisted with modeling, sampling and laboratory analyses; JJ and GL assisted with modeling and data processing; CL was in charge of the whole trial. All authors read and approved the final manuscript.

Author's Information
Dexiang Wang, born in 1988, is currently an associate professor and a master's supervisor at *School of Mechanical and Automotive Engineering, Qingdao University of Technology, China*. His main research interests include grinding and controlled manufacture of rolling bearing raceway.
Yu Zhang, born in 1997, is currently a master candidate at *Qingdao University of Technology, China*.
Qiliang Zhao, born in 1995, is currently a graduated master student from *Qingdao University of Technology, China*.
Jingliang Jiang, born in 1982, is currently an associate professor and a master's supervisor at *School of Mechanical and Automotive Engineering, Qingdao University of Technology, China*. His main research interests include grinding and tribology.
Guoliang Liu, born in 1990, is currently an associate professor and a master's supervisor at *School of Mechanical and Automotive Engineering, Qingdao University of Technology, China*. His main research interests include green manufacture and high-efficiency machining.
Changhe Li, born in 1966, is currently a professor and a PhD candidate supervisor at *School of Mechanical and Automotive Engineering, Qingdao University of Technology, China*. His main research interests include precision machining and green manufacturing.

Funding
Supported by Shandong Provincial Natural Science Foundation of China (Grant Nos. ZR2022ME208, ZR2020QE181), National Natural Science Foundation of China (Grant Nos. 51705272, 52005281), China Postdoctoral Science Foundation (Grant No. 2018M642628), and 111 project (Grant No. D21017).

Availability of data and materials
The datasets supporting the conclusions of this article are included within the article.

Declarations

Ethics approval and consent to participate
Not applicable.

Consent for publication
Not applicable.

Competing interests
The authors declare no competing financial interests.

Author Details
[1]School of Mechanical and Automotive Engineering, Qingdao University of Technology, Qingdao, China. [2]Key Lab of Industrial Fluid Energy Conservation and Pollution Control (Qingdao University of Technology), Ministry of Education, Qingdao, China.

Received: 15 July 2022 Revised: 3 May 2023 Accepted: 4 May 2023
Published online: 30 June 2023

References
[1] M N Morgan, A R Jackson, H Wu, et al. Optimisation of fluid application in grinding. *CIRP Annals - Manufacturing Technology*, 2008, 57(1): 363-366.
[2] J Sieniawski, K Nadolny. The effect upon grinding fluid demand and workpiece quality when an innovative zonal centrifugal provision method is implemented in the surface grinding of steel CrV12. *Journal of Cleaner Production*, 2016, 113: 960-972.
[3] A Shokrani, V Dhokia, S T Newman. Environmentally conscious machining of difficult-to-machine materials with regard to cutting fluids. *International Journal of Machine Tools and Manufacture*, 2012, 57: 83-101.
[4] M Hadad, B Sadeghi. Thermal analysis of minimum quantity lubrication-MQL grinding process. *International Journal of Machine Tools and Manufacture*, 2012, 63: 1-15.
[5] Y B Zhang, C H Li, M Yang, et al. Experimental evaluation of cooling performance by friction coefficient and specific friction energy in nanofluid minimum quantity lubrication grinding with different types of vegetable oil. *Journal of Cleaner Production*, 2016, 139: 685-705.
[6] Y B Zhang, C H Li, D Z Jia, et al. Experimental study on the effect of nanoparticle concentration on the lubricating property of nanofluids for MQL grinding of Ni-based alloy. *Journal of Materials Processing Technology*, 2016, 232: 100-115.
[7] X Bai, J Jiang, C Li, et al. Tribological performance of different concentrations of Al_2O_3 nanofluids on minimum quantity lubrication milling. *Chinese Journal of Mechanical Engineering*, 2023, 36: 11.
[8] B Fang, J Zhang, J Hong, et al. Research on the nonlinear stiffness characteristics of double-row angular contact ball bearings under different working conditions. *Lubricants*, 2023, 11(2): 44.
[9] Y G Wang, C H Li, Y B Zhang, et al. Experimental evaluation of the lubrication properties of the wheel/workpiece interface in MQL grinding with different nanofluids. *Tribology International*, 2016, 99: 198-210.
[10] Y G Wang, C H Li, Y B Zhang, et al. Experimental evaluation on tribological performance of the wheel/workpiece interface in minimum quantity lubrication grinding with different concentrations of Al_2O_3 nanofluids. *Journal of Cleaner Production*, 2016, 142: 3571-3583.
[11] S J Ma, Y J Yin, B Chao, et al. A real-time coupling model of bearing-rotor system based on semi-flexible body element. *International Journal of Mechanical Sciences*, 2023, 245: 108098.
[12] Y S Dambatta, M Sayuti, A Sarhan, et al. Tribological performance of SiO_2-based nanofluids in minimum quantity lubrication grinding of Si_3N_4 ceramic. *Journal of Manufacturing Processes*, 2019, 41: 135-147.
[13] R L Virdi, S S Chatha, H Singh. Performance evaluation of nanofluid-based minimum quantity lubrication grinding of Ni-Cr alloy under the influence of CuO nanoparticles. *Advances in Manufacturing*, 2021, 9(4): 580-591.
[14] A Azami, Z Salahshournejad, E Shakouri, et al. Influence of nano-minimum quantity lubrication with MoS_2 and CuO nanoparticles on cutting forces and surface roughness during grinding of AISI D2 steel. *Journal of Manufacturing Processes*, 2023, 87: 209-220.
[15] M Wang, K Yan, Q Tang, et al. Dynamic modeling and properties analysis for ball bearing driven by structure flexible deformations. *Tribology International*, 2023, 179: 108163.
[16] B Shen, P Kalita, A P Malshe, et al. Performance of novel MoS_2 nanoparticles based grinding fluids in minimum quantity lubrication grinding. *Transactions of NAMRI/SME*, 2008, 36(357): 357-364.
[17] D Wang, Y Zhang, Q Zhao, et al. Tribological mechanism of carbon group nanofluids on grinding interface under minimum quantity lubrication based on molecular dynamics simulation. *Frontiers of Mechanical Engineering*, 2023, 18(1): 17.
[18] B Shen, A J Shih, S C Tung. Application of nanofluids in minimum quantity lubrication grinding. *Tribology Transactions*, 2008, 51: 730-737.
[19] T Gao, C H Li, D Z Jia, et al. Surface morphology assessment of CFRP transverse grinding using CNT nanofluid minimum quantity lubrication. *Journal of Cleaner Production*, 2020, 277: 123328.
[20] R B Pavan, A V Gopal, M Amrita, et al. Experimental investigation of graphene nanoplatelets-based minimum quantity lubrication in grinding Inconel 718. *Proceedings of the Institution of Mechanical Engineers Part B: Journal of Engineering Manufacture*, 2019, 233: 400-410.
[21] A M M Ibrahim, W Li, H Xiao, et al. Energy conservation and environmental sustainability during grinding operation of Ti-6Al-4V alloys via eco-friendly oil/graphene nano additive and Minimum quantity lubrication. *Tribology International*, 2020, 150: 106387.
[22] H Singh, V S Sharma, M Dogra. Exploration of graphene assisted vegetables oil based minimum quantity lubrication for surface grinding of TI-6AL-4V-ELI. *Tribology International*, 2020, 144: 106113.
[23] M Li, T Yu, R Zhang, et al. Experimental evaluation of an eco-friendly grinding process combining minimum quantity lubrication and graphene-enhanced plant-oil-based cutting fluid. *Journal of Cleaner Production*, 2020, 244: 118747.
[24] A A Balandin, S Ghosh, W Bao, et al. Superior thermal conductivity of single-layer graphene. *Nano Letters*, 2008, 8: 902-907.

[25] J B Pu, L P Wang, Q J Xue. Progress of tribology of graphene and graphene-based composite lubricating materials. *Tribology*, 2014, 34: 93-112.
[26] C Lee, X Wei, J W Kysar, et al. Measurement of the elastic properties and intrinsic strength of monolayer graphene. *Science*, 2008, 321: 385-388.
[27] M E Van Valkenburg, R L Vaughn, M Williams, et al. Thermochemistry of ionic liquid heat-transfer fluids. *Thermochimica Acta*, 2005, 425: 181-188.
[28] F Wang. *Thermophysical property and solar-thermal convertion efficiency of graphene/ionic liquid nanofluids for solar collectors*. Guangzhou: South China University of Technology, 2013. (in Chinese)
[29] J F Hoffmann, G Vaitilingom, J F Henry, et al. Temperature dependence of thermophysical and rheological properties of seven vegetable oils in view of their use as heat transfer fluids in concentrated solar plants. *Solar Energy Materials and Solar Cells*, 2018, 178: 129-138.
[30] Qingdao Ionike New Material Technology Co., Ltd. 1-butyl-3-methylimidazolium tetrafluoroborate [EB/OL]. http://www.ionike.com/product/Imidazolium/MIm/2014-03-27/23.html. Accessed 27 March 2014.
[31] Qingdao Ionike New Material Technology Co., Ltd. 1-hexyl-3-methylimidazolium tetrafluoroborate [EB/OL]. http://www.ionike.com/product/Imidazolium/MIm/2014-03-28/45.html. Accessed 28 March 2014.
[32] J Dweck, C M S Sampaio. Analysis of the thermal decomposition of commercial vegetable oils in air by simultaneous TG/DTA. *Journal of Thermal Analysis and Calorimetry*, 2004, 75: 385-391.
[33] M Cai, Q Yu, W Liu, et al. Ionic liquid lubricants: When chemistry meets tribology. *Chemical Society Reviews*, 2020, 49: 7753-7818.
[34] M Q Pham, H S Yoon, V Khare, et al. Evaluation of ionic liquids as lubricants in micro milling–process capability and sustainability. *Journal of Cleaner Production*, 2014, 76: 167-173.
[35] G S Goindi, A D Jayal, P Sarkar. Application of ionic liquids in interrupted minimum quantity lubrication machining of plain medium carbon steel: Effects of ionic liquid properties and cutting conditions. *Journal of Manufacturing Processes*, 2018, 32: 357-371.
[36] I Del Sol, A J Gámez, A Rivero, et al. Tribological performance of ionic liquids as additives of water-based cutting fluids. *Wear*, 2019, 426: 845-852.
[37] A K Singh, A Kumar, V Sharma, et al. Sustainable techniques in grinding: A review. *Journal of Cleaner Production*, 2020, 269: 121876.
[38] X Wang, Y Song, C Li, et al. Nanofluids application in machining: A comprehensive review. *International Journal of Advanced Manufacturing Technology*, 2023. https://doi.org/10.1007/s00170-022-10767-2
[39] X Cui, C Li, W Ding, et al. Minimum quantity lubrication machining of aeronautical materials using carbon group nanolubricant: from mechanisms to application. *Chinese Journal of Aeronautics*, 2022, 35(11): 85-112.
[40] Y Zhang, H Li, C Li, et al. Nano-enhanced biolubricant in sustainable manufacturing: from processability to mechanisms. *Friction*, 2022, 10(6): 803-841.
[41] D X Wang, S F Sun, Y Z Tang, et al. Molecular dynamics simulation for grinding interface under minimum quantity lubrication. *Journal of Xi'an Jiaotong University*, 2020, 54: 168-175. (in Chinese)
[42] D X Wang, Q L Zhao, Y Zhang, et al. Investigation on tribological mechanism of ionic liquid on grinding interfaces under MQL. *China Mechanical Engineering*, 2022, 33(05): 560-568. (in Chinese)
[43] M J Hadad, T Tawakoli, M H Sadeghi, et al. Temperature and energy partition in minimum quantity lubrication-MQL grinding process. *International Journal of Machine Tools and Manufacture*, 2012, 54: 10-17.
[44] Y Hua. *Residual stress and fatigue life of machined superalloy GH4169 with turning-burnishing successive process*. Jinan: Shandong University, 2020. (in Chinese)
[45] Y H Fan, W Y Wang, Z P Hao, et al. Work hardening mechanism based on molecular dynamics simulation in cutting Ni–Fe–Cr series of Ni-based alloy. *Journal of Alloys and Compounds*, 2020, 819: 153331.
[46] Y Zhang, C Li, D Jia, et al. Experimental evaluation of the lubrication performance of MoS_2/CNT nanofluid for minimal quantity lubrication in Ni-based alloy grinding. *International Journal of Machine Tools and Manufacture*, 2015, 99: 19-33.
[47] P Vashishta, R K Kalia, A Nakano, et al. Interaction potentials for alumina and molecular dynamics simulations of amorphous and liquid alumina. *Journal of Applied Physics*, 2008, 103(8): 083504.
[48] G Bonny, D Terentyev, R C Pasianot, et al. Interatomic potential to study plasticity in stainless steels: the FeNiCr model alloy. *Modelling and Simulation in Materials Science and Engineering*, 2011, 19(8): 085008.
[49] Z Liu, S Huang, W Wang. A refined force field for molecular simulation of imidazolium-based ionic liquids. *The Journal of Physical Chemistry B*, 2004, 108(34): 12978-12989.
[50] Z P Hao, X Han, Y H Fan. Molecular dynamics analysis of tool wear in cutting Ni-Fe-Cr-Co-Cu based nickel alloys. *Mechanical Engineering and Technology*, 2020, 9(2): 60-68.
[51] J Tersoff. Empirical interatomic potential for silicon with improved elastic properties. *Physical Review B*, 1988, 38(14): 9902-9905
[52] X Chang. Ripples of multilayer graphenes: A molecular dynamics study. *Acta Physica Sinica*, 2014, 63(08): 336-341.
[53] T Liang, P Zhang, P Yuan, et al. In-plane thermal transport in black phosphorene/graphene layered heterostructures: A molecular dynamics study. *Physical Chemistry Chemical Physics*, 2018, 20(32): 21151-21162.
[54] X H Liu, X W Lu, N R He, et al. Influence of annealing temperature on structure and high temperature tribological properties of chromium oxide films. *Tribology*, 2019, 39(02): 164-170.
[55] J F Sun, A S Li, F H Su, et al. Tribological property of titanium alloy surface with different texture structure under dry friction and perfluoropolyether lubrication. *Tribology*, 2018, 38(6): 658-664.
[56] S H Choa, K C Ludema, G E Potter. A model for the boundary film formation and tribological behavior of a phosphazene lubricant on steel. *Tribology Transactions*, 1995, 38(4): 757-768.